



Article

Green-Light GaN p-n Junction Luminescent Particles Enhance the Superconducting Properties of B(P)SCCO Smart Meta-Superconductors (SMSCs)

Qingyu Hai, Honggang Chen, Chao Sun, Duo Chen, Yao Qi, Miao Shi and Xiaopeng Zhao *

Smart Materials Laboratory, Department of Applied Physics, Northwestern Polytechnical University, Xi'an 710129, China; haiqingyu@mail.nwpu.edu.cn (Q.H.); 2017100698@mail.nwpu.edu.cn (H.C.); znclsunc.nwpu.edu.cn@mail.nwpu.edu.cn (C.S.); chenduo@mail.nwpu.edu.cn (D.C.); qiyao@mail.nwpu.edu.cn (Y.Q.); shimiao@mail.nwpu.edu.cn (M.S.)

* Correspondence: xpzhao@nwpu.edu.cn

Abstract: Superconducting materials exhibit unique physical properties and have great scientific value and vast industrial application prospects. However, due to limitations, such as the critical temperature (T_C) and critical current density (J_C), the large-scale application of superconducting materials remains challenging. Chemical doping has been a commonly used method to enhance the superconductivity of B(P)SCCO. However, satisfactory enhancement results have been difficult to achieve. In this study, we introduce green-light GaN p-n junction particles as inhomogeneous phases into B(P)SCCO polycrystalline particles to form a smart meta-superconductor (SMSC) structure. Based on the electroluminescence properties of the p-n junction, the Cooper pairs were stimulated and strengthened to enhance the superconductivity of B(P)SCCO. The experimental results demonstrate that the introduction of inhomogeneous phases can indeed enhance the critical temperature T_C , critical current density J_C , and complete diamagnetism (Meissner effect) of B(P)SCCO superconductors. Moreover, when the particle size of the raw material of B(P)SCCO is reduced from 30 to 5 μm , the grain size of the sintered samples also decreases, and the optimal doping concentration of the inhomogeneous phases increases from 0.15 wt.% to 0.2 wt.%, further improving the superconductivity.

Keywords: B(P)SCCO; smart superconductors (SMSCs); inhomogeneous phase of p-n junction particles; electroluminescence properties; enhancement of superconductivity



Citation: Hai, Q.; Chen, H.; Sun, C.; Chen, D.; Qi, Y.; Shi, M.; Zhao, X.

Green-Light GaN p-n Junction Luminescent Particles Enhance the Superconducting Properties of B(P)SCCO Smart Meta-Superconductors (SMSCs).

Nanomaterials **2023**, *13*, 3029.

<https://doi.org/10.3390/nano13233029>

nano13233029

Academic Editor: Erik Piatti

Received: 2 November 2023

Revised: 24 November 2023

Accepted: 25 November 2023

Published: 27 November 2023



Copyright: © 2023 by the authors. Licensee MDPI, Basel, Switzerland. This article is an open access article distributed under the terms and conditions of the Creative Commons Attribution (CC BY) license (<https://creativecommons.org/licenses/by/4.0/>).

1. Introduction

Superconducting materials have attracted widespread attention in the scientific community due to their unique physical properties, such as zero electrical resistance [1] and complete diamagnetism [2]. However, the low-current carrying density and the requirement for low-temperature environments during operation limit the practical applications of superconducting materials to some extent. Therefore, the discovery of new superconducting materials and the continuous improvements of the critical temperature (T_C) and critical current density (J_C) are ongoing goals in the scientific community in order to create room-temperature superconductors. Since the 1980s, with the discovery of cuprate [3,4] and iron-based superconductors [5–7], the critical temperature (T_C) has surpassed the McMillan limit (40 K) and reached the liquid nitrogen temperature range (70 K). The development of superconducting materials has entered the high-temperature superconductivity phase, greatly inspiring researchers' confidence. To date, nearly a hundred types of superconducting materials have been discovered, but the progress in increasing the critical temperature (T_C) remains slow.

In recent years, researchers have also discovered emerging superconducting materials, such as high-pressure [8–11], photoinduced [12–14], 2D [15–17], interfacial [18–20], and nickel-based superconductors [21–23]. In 2019, a team from Stanford University in the

United States discovered superconductivity in a $\text{Nd}_{0.8}\text{Sr}_{0.2}\text{NiO}_2$ thin-film material, with a critical temperature (T_C) of approximately 15 K [21]. In 2021, Xie et al. found superconductivity at the interface of KTaO_3 and LaAlO_3 crystals, with a critical temperature (T_C) of around 2.2 K, and achieved the transition between the superconducting and insulating phases under electric field control [23]. In July 2023, Wang Meng et al. from Sun Yat-sen University reported the emergence of superconductivity in $\text{La}_3\text{Ni}_2\text{O}_7$ single-crystal samples under a pressure of 14 GPa, with a critical temperature (T_C) of 80 K [23]. These superconducting materials cannot be further applied at the moment, but they greatly help us to further explore superconducting materials and investigate the mechanisms behind the generation of superconductivity.

Although progress in increasing the critical temperature (T_C) of superconducting materials has been slow, we still have not created low-cost superconductors. However, with the development of science and technology, superconducting materials play an increasingly important role in fields, such as electric grids [24], energy [25], healthcare [26], controlled nuclear fusion [27], and quantum computing [28–30]. Based on the zero-resistance property of superconductors, high-temperature superconducting wires, like BSCCO, YBCO, and REBCO, have been made into superconducting cables for power transmission [31–33]. Nb-based alloys, known for their high critical current density (J_C), high critical magnetic field (H_C), and low manufacturing cost, are used to produce superconducting magnets with low Joule and magnetic losses, serving as important components in nuclear magnetic resonance imaging devices, tokamak devices, or superconducting rotating machines [34,35]. Iron-based superconductors, with their high H_C characteristics, also play an increasingly important role in high-magnetic-field applications [36,37].

A BSCCO superconductor is a typical copper oxide superconductor, consisting of three coexisting superconducting phases, Bi-2201 ($T_C = 20$ K), Bi-2212 ($T_C = 87$ K), and Bi-2223 ($T_C = 110$ K), all of which have a cubic crystal structure [38–41]. This structure can be seen as a pseudo-perovskite layered structure, where the CuO_2 layers serve as the intrinsic superconducting layer and the BiO, SrO, and Ca atomic layers alternate as charge reservoir layers [4,42]. The charge reservoir layers generate charge carriers, which transfer to the superconducting layer at the interface, thus maintaining the purity of the superconducting layer to some extent and reducing impurity scattering, facilitating macroscopic superconductivity. Furthermore, this structure can be viewed as a natural Josephson junction, and it has been proposed by researchers that BSCCO superconductors can be used to fabricate terahertz wave emitters based on the ac Josephson effect [43–45]. BSCCO superconductors have the characteristics of not containing rare-earth elements, a high critical temperature (T_C), insensitivity to oxygen, and simple manufacturing process, making them the most widely used and promising superconducting materials in industrial applications. Enhancing the superconducting properties of BSCCO superconductors can not only further enhance the application value of BSCCO, but also contribute to our exploration and understanding of superconducting mechanisms. To date, the most common method to enhance the superconducting properties of BSCCO superconductors is chemical doping, such as doping elements like Pb [46], Al [47], Cs [48], and Ce [49] into BSCCO superconductors to improve their performance through element substitution. Studies have shown that, in the case of Pb doping, where Pb^{2+} partially replaces Bi^{3+} , the structure of the Bi-2223 phase becomes more stable and the content of the Bi-2223 phase is increased, but the critical temperature (T_C) cannot be improved. Similarly, doping with Al, Cs, Ce, and other elements cannot increase T_C , but it can effectively enhance the critical current density (J_C) at proper doping concentrations. Alternatively, doping compounds like Al_2O_3 [50], SnO_2 [51], ZrO_2 [52], and MgO [53] into BSCCO superconductors cannot increase T_C , and in some cases, it may even decrease T_C , but at appropriate doping concentrations, J_C can be effectively enhanced. Thus, it can be seen that the results of chemical doping methods are not ideal and cannot effectively increase T_C and J_C .

Metamaterial is a kind of composite material with an artificial structure, allowing for the realization of unique or even non-existent “anomalous” material properties in nature [54–56]. Based on metamaterial methods, our research team proposed a new type of smart superconducting material called smart meta-superconductors (SMSCs). Superconducting polycrystalline particles are used as the matrix, and electroluminescent particles are introduced as the inhomogeneous phase into the superconducting polycrystalline particles, forming the structure of the SMSCs. In previous studies, we introduced $Y_2O_3:Eu^{3+}$ and $Y_2O_3:Eu^{3+} + Ag$ electroluminescent materials as the inhomogeneous phase into MgB_2 [57–60] and B(P)SCCO [61–63] superconductors, forming smart meta-superconductors. We believe that this structure can treat superconducting particles as microelectrodes. When a current is applied, the electroluminescence of the inhomogeneous phase is excited by the electric field between the microelectrodes, stimulating and enhancing Cooper pairs, thereby improving the superconducting properties. Research has shown that this type of SMSC material, which can be modulated and improved in superconducting properties by an external field stimulation, possesses new characteristics that traditional chemical doping methods cannot achieve. When measuring the T_C of SMSCs using the four-probe method, the external electric field stimulates the electroluminescence of the inhomogeneous phase (EL), thereby enhancing the Cooper pairs and increasing the critical temperature T_C . However, $Y_2O_3:Eu^{3+}$ and $Y_2O_3:Eu^{3+} + Ag$ electroluminescent materials require a strong electric field stimulation, and the low and unstable luminous intensity easily decays, which cannot effectively enhance the critical temperature T_C . In recent years, our team also introduced red AlGaInP p-n junction particles as the inhomogeneous phase into conventional MgB_2 superconductors, forming smart meta-superconductors [64]. The results show that, compared to $Y_2O_3:Eu^{3+}$ and $Y_2O_3:Eu^{3+} + Ag$ electroluminescent materials, p-n junction particles can more effectively enhance the critical temperature T_C , critical current density J_C , and complete diamagnetism (Meissner effect) of MgB_2 superconductors due to their structural stability, high luminous intensity, and the ability to be activated at a low voltage.

The successful incorporation of red AlGaInP p-n junctions as inhomogeneous phases into conventional superconductor MgB_2 to form smart meta-superconductors raises the question of whether it is equally effective for high-temperature superconductors. In this paper, we investigate the doping of green-light GaN p-n junction particles as inhomogeneous phases into high-temperature B(P)SCCO superconductors, forming smart material superconductors. The study demonstrates that the doping of p-n junction nanostructures ensures the stability of material performance and effectively enhances the critical temperature T_C , critical current density J_C , and complete diamagnetism (Meissner effect) of B(P)SCCO superconductors. Furthermore, as the particle size of the B(P)SCCO polycrystalline particles decreases with the reduction in the raw material particle size, the doping content of the p-n junction inhomogeneous phase increases, further amplifying the enhancement effect on the superconducting properties.

2. Model

Figure 1 illustrates the concept of using metamaterials to construct a smart meta-superconductor model, based on polycrystalline B(P)SCCO as the matrix. The gray rectangles in the image represent polycrystalline B(P)SCCO particles. The green particles are GaN p-n junction luminescent particles that emit green light waves with a central wavelength of 550 nm, and they are dispersed as inhomogeneous phases around the polycrystalline B(P)SCCO particles. When measuring the sample’s performance, under the influence of an external electric field, the superconductor polycrystalline particles serve as microelectrodes, effectively exciting electroluminescence in the inhomogeneous phase, thereby stimulating Cooper pairs and enhancing superconducting properties. In addition, as the size of B(P)SCCO polycrystalline particles decreases, more inhomogeneous phases can be accommodated within the same spatial volume, further increasing the enhancement effect of superconductivity.

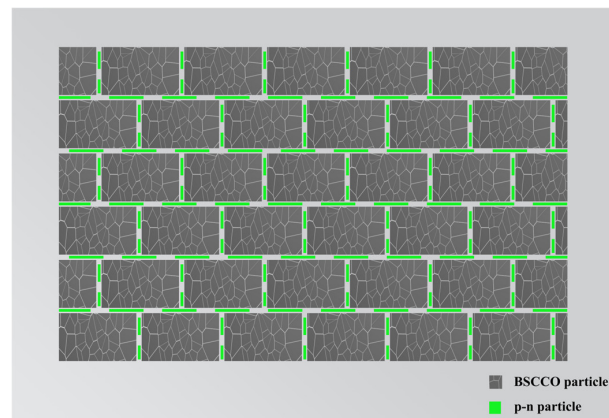


Figure 1. Diagram of the B(P)SCCO SMSCs model.

3. Materials and Methods

3.1. Preparation of p-n Junction Luminescent Particles

The raw material used was a commercial green-light LED epitaxial wafer (Xiamen Qianzhao Optoelectronics Co., Ltd., Xiamen, China), with GaN as the main component and an emission wavelength of 550 nm. It was grown on a sapphire substrate using the metal-organic chemical vapor deposition method, with the activation temperature of the p-type layer exceeding 1300 °C. The p-n junction luminescent structure was detached from the Al₂O₃ substrate and mechanically ground to obtain p-n junction luminescent particles measuring 2 μm × 2 μm × 1.7 μm, as shown in the SEM diagram in Figure 2a. Figure 2b shows the statistical distribution of the particle sizes of the p-n junction particles. It can be observed from the figure that the particle sizes of the p-n junction particles are concentrated in the range of 1–2 μm, with an average size of 1.5 μm. The p-n junction particles ground from the substrate has a three-layer nanostructure of an n-type GaN semiconductor, multi-quantum well, and p-type GaN semiconductor. GaN is a stable compound with a melting point of 1700 °C, so the p-n junction particles can withstand long-term annealing at 840 °C. The GaN p-n junction particles can emit light when a voltage of <10 V and a current of <10 mA are applied; therefore, during the sample testing, the testing current was used to illuminate the p-n junction particles. Figure 2c shows the brightness graph of the p-n junction particles illuminated at a voltage of <10 V and a current of <10 mA. The green curve represents the brightness of the p-n junction particles, while the red curve represents the brightness of Y₂O₃:Eu³⁺ + Ag rare-earth oxide electroluminescent particles prepared by our team [65]. It can be seen from the graph that the brightness of the p-n junction luminescent particles is much greater than that of the Y₂O₃:Eu³⁺ + Ag rare-earth oxide electro-luminescent particles. Moreover, the p-n junction luminescent particles can maintain continuous luminescence for more than 1000 h without brightness decay, indicating a superior luminescent performance compared to the Y₂O₃:Eu³⁺ + Ag rare-earth oxide electroluminescent particles.

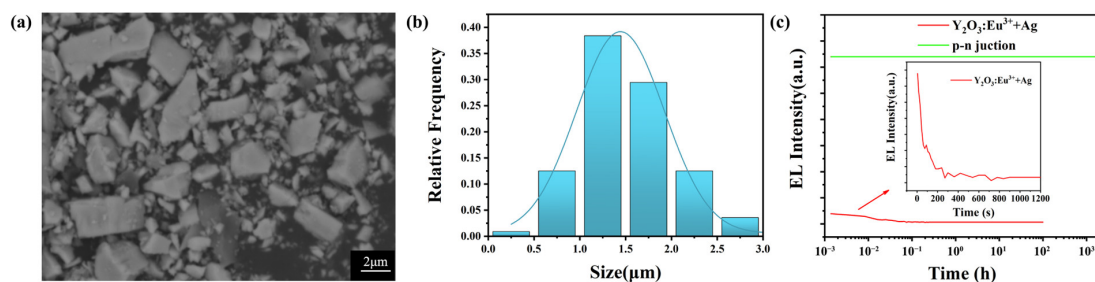


Figure 2. (a) SEM diagram of p-n junction particles, ground into 2 μm × 2 μm × 1.7 μm particles; (b) particle size distribution of the p-n junction particles; (c) luminescence intensity and lifetime test curves of p-n junction particles and rare-earth oxide particles in red-light wavelengths.

3.2. Preparation of B(P)SCCO Precursor Powders

Certain amounts of Bi_2O_3 (Alfa Aesar, Haverhill, MA, USA, 99.99%), PbO (Alfa Aesar, 99.99%), SrCO_3 (Alfa Aesar, 99.99%), CaCO_3 (Alfa Aesar, 99.99%), and CuO (Alfa Aesar, 99.99%) powders were weighed according to the molar ratio of 1.6:0.4:2:2:3. The mixed raw powders were placed in a 50 mL ball milling jar with anhydrous ethanol as the grinding aid, and the ball milling machine was set at a speed of 500 rpm for 20 or 80 h. The raw materials milled for 20 h were dried and sieved through a 500 mesh stainless-steel sieve to obtain the raw material S1 with a particle size of about 30 μm . The raw materials milled for 80 h were filtered and dried using a G4 funnel, and then we obtained the raw material S2 with a particle size of about 5 μm . The raw materials S1 and S2 were separately placed in a tube furnace and annealed at 840 $^\circ\text{C}$ in air for 50 h + 50 h. After intermediate grinding, two different-sized black B(P)SCCO precursor powders were obtained.

3.3. Preparation of BSCCO Superconductor and Inhomogeneous Phase Sample

A certain amount of B(P)SCCO precursor powder was weighed and placed in a mold. The powder was pressed under a pressure of 12 MPa for 10 min to form a circular disk with a diameter of 12 mm and a thickness of 1 mm. The disk was then placed in a ceramic boat. The ceramic boat was transferred to a tube furnace and annealed at a temperature of 840 $^\circ\text{C}$ for 30 h. After cooling to room temperature, the disk was removed from the ceramic boat and thoroughly ground into powder. The ground B(P)SCCO powder and the corresponding inhomogeneous phase p-n junction particles with different mass fractions were placed in separate beakers and mixed with anhydrous ethanol to form a solution. The two solutions were then transferred to an ultrasonic cleaner and sonicated for 20 min. After sonication, the solutions were placed on a magnetic stirrer. During the stirring process, the inhomogeneous phase solution was added dropwise to the B(P)SCCO solution using a pipette. After completion, the mixture was stirred for 10 min and sonicated for 20 min. The mixed solution was then transferred to a Petri dish and placed in a vacuum drying oven. The sample was dried at 65 $^\circ\text{C}$ under vacuum for 5 h to obtain a black powder. The dried B(P)SCCO black powder was placed in a mold and pressed under a pressure of 12 MPa for 10 min to form a circular disk with a diameter of 12 mm and a thickness of 1 mm. The disk was then placed in a ceramic boat. The ceramic boat was transferred to a tube furnace and annealed at a temperature of 840 $^\circ\text{C}$ in an air atmosphere for 120 h. After cooling to room temperature, the corresponding sample was obtained.

Samples created using raw material S1 are referred to as the A series, while samples created using raw material S2 are referred to as the B series. The sample numbers and doping concentrations of the A- and B-series samples are shown in Tables 1 and 2, respectively.

Table 1. Sample numbers and doping concentrations of the A-series samples prepared using raw material S1 (30 μm).

Samples	A1	A2	A3	A4
Inhomogeneous phase p-n junction concentration (wt.%)	0	0.1	0.15	0.2

Table 2. Sample numbers and doping concentrations of the B-series samples prepared using raw material S2 (5 μm).

Samples	B1	B2	B3	B4	B5
Inhomogeneous phase p-n junction concentration (wt.%)	0	0.1	0.15	0.2	0.25

3.4. Measurement of Critical Temperature (T_c)

The resistance–temperature dependence (R–T) curves of the prepared samples at low temperatures were measured using the four-probe method to determine the zero-resistance transition temperature ($T_{C,0}$) and the onset transition temperature ($T_{C,on}$) of the samples. The entire testing process was conducted under vacuum conditions, with a closed-cycle cryostat provided by Advanced Research Systems to create the low-temperature environment (minimum temperature of 10 K). The temperature during the testing process was controlled by a low-temperature controller from Lake Shore. The high-temperature superconducting material characteristic testing system produced by Shanghai Qianfeng Electronic Instrument Co., Ltd. (Shanghai, China) provided the testing current (0.1–100 mA), and the voltage measurement was performed using a Keithley digital nanovoltmeter.

3.5. Measurement of Critical Current Density and Meissner Effect

The measurement of current–voltage (I–V) characteristics under zero-magnetic-field conditions was also performed using the four-probe method. The sample was connected to the leads using indium wire, and a certain current level was applied to the sample through the outermost two leads, while the voltage was measured using a Keithley digital nanovoltmeter connected to the middle two leads. When the current flowing through the sample, denoted as I , exceeded a certain threshold, the superconducting state of the sample was disrupted and transitioned to the normal state. This critical current is known as the critical transport current of the superconductor. Typically, the critical transport current density (J_c) in a superconducting system is determined by measuring the I–V characteristics at different temperatures (below the onset transition temperature, $T_{C,on}$), with a voltage criterion of $1 \mu\text{V}/\text{cm}$. During the testing process, the shape and size of all samples, as well as the distances between the current and voltage leads, were kept constant. Subsequently, DC magnetization testing was performed on the prepared samples. The samples were slowly cooled in a 2.5 mT magnetic field parallel to the plane, and the data were collected during the subsequent warming process. All samples exhibited complete diamagnetism.

4. Results

4.1. Scanning Electron Microscope (SEM)

Figure 3 shows the SEM images of the pure B(P)SCCO samples A1 (Figure 3a) and B1 (Figure 3c) prepared from raw materials S1 and S2, respectively. From the images, it can be observed that all samples exhibit a randomly distributed layered structure. Figure 3b,d show the statistical distribution of the size of the layered structure in samples A1 and B1, respectively. It can be observed from the figures that the size distribution of the layered structure in sample A1 ranges from 2.5 to 7.5 μm , with an average size of 5 μm . The size distribution of the layered structure in sample B1 ranges from 1 to 4 μm , with an average size of 2.5 μm . The layered structure of sample B1 is smaller in size and contains more gaps compared to sample A1. This indicates that, as the size of the raw materials decreases, the particle size of the prepared samples decreases while the gaps between the particles increase. Therefore, under the same volume, more p-n junction luminescent inhomogeneous phases can be accommodated. Figure 4a shows the SEM image of the B(P)SCCO sample (A3) doped with 0.15 wt.% p-n junction luminescent inhomogeneous phases. It can be observed that the introduction of p-n junction luminescent inhomogeneous phases does not seem to have a significant impact on the size of the sample's layered structure or the connectivity between particles. Figure 4b–f show the EDS mapping images for elements Bi, Sr, Ca, Cu, and Ga listed in the top-right corner of each figure. It indicates that the GaN p-n junction luminescent particles are randomly distributed around the B(P)SCCO layered structure.

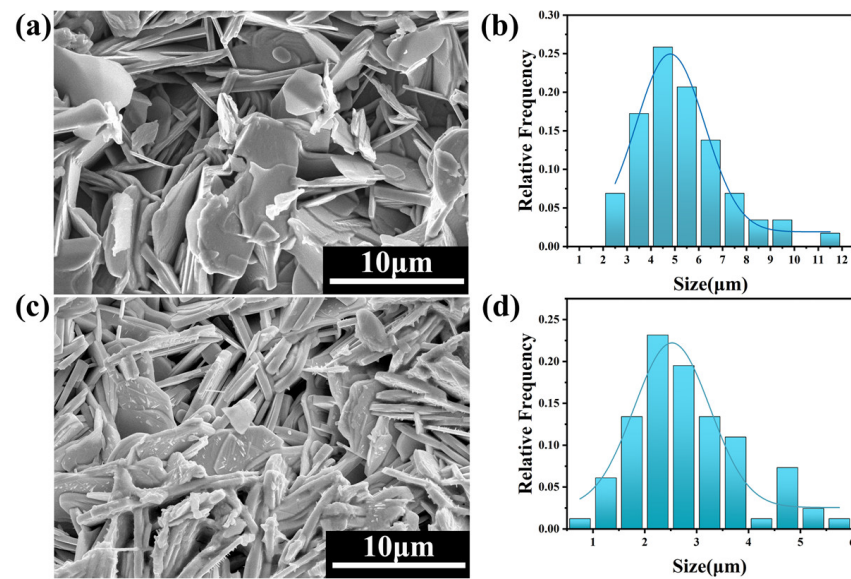


Figure 3. SEM diagram of the pure samples A1 (a) and B1 (c) prepared from the raw materials S1, S2 after sintering, and the distribution of the size of the layered structure in samples A1 (b) and B1 (d).

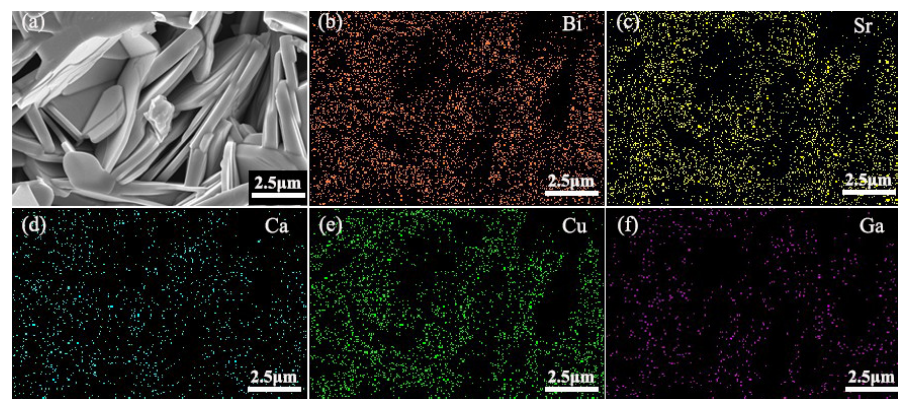


Figure 4. (a) SEM diagram of the sample (A3) after sintering; (b–f) EDS mapping of Bi, Sr, Ca, Cu, and Ga.

4.2. Critical Temperature T_C

Table 3 and Figure 5a show the critical temperature (T_C) and normalized R–T curves of the A-series samples prepared from raw material S1 with a particle size of 30 μm , as measured by the four-probe method. The black curve in the figure represents the pure sample A1 of B(P)SCCO, with a transition temperature of 103–114 K. The remaining three curves represent the inhomogeneous phase-doped samples A2, A3, and A4 with x wt.% ($x = 0.1, 0.15, 0.2$) content, with transition temperatures of 103.5–114, 105–114, and 104–114 K, respectively. Figure 5b shows the zero-resistance transition temperature $T_{C,0}$ of the A-series samples. Figure 5c shows the enhancement of the zero-resistance transition temperature ($T_{C,0}$) in the A-series samples, denoted as $\Delta T_{C,0}$. It can be observed from the figure that the inhomogeneous phase doping effectively enhances the zero-resistance transition temperature $T_{C,0}$ of the B(P)SCCO superconductor, and the enhancement $\Delta T_{C,0}$ shows a normal distribution relationship with the content of inhomogeneous phase doping. The optimal doping content is 0.15 wt.% and the zero-resistance transition temperature $T_{C,0}$ is increased by 2 K.

Table 3. Critical temperature (T_C) of A-series samples.

Samples	Concentration (wt.%)	$T_{C,0}/K$	$T_{C,on}/K$	$\Delta T_{C,0}/K$	$\Delta T_{C,on}/K$	Transition Width/K
A1	0	103 ± 0.17	114 ± 0.15	0	0	11
A2	0.1	103.5 ± 0.11	114 ± 0.13	0.5	0	10.5
A3	0.15	105 ± 0.19	114 ± 0.16	2	0	9
A4	0.2	104 ± 0.16	114 ± 0.17	1	0	10

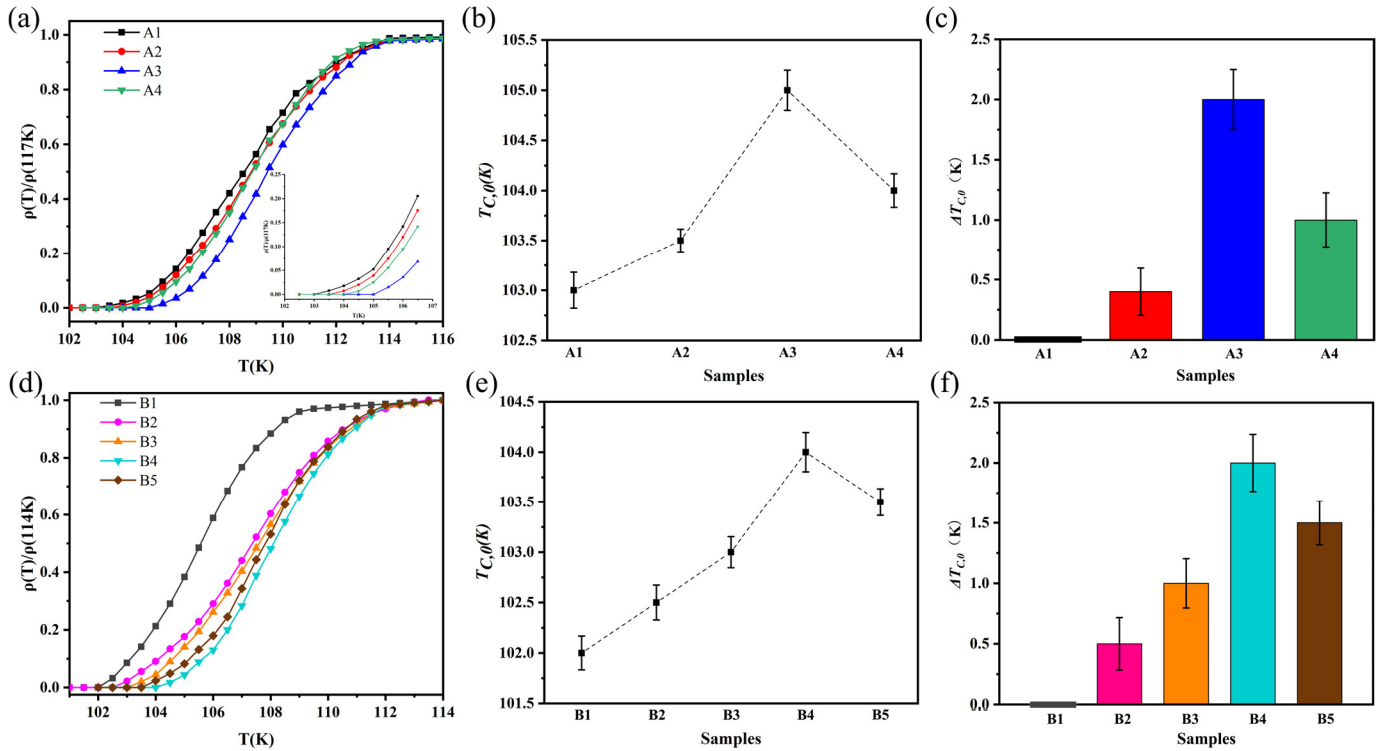


Figure 5. (a) Normalized R–T curve of A-series samples; (b) zero-resistance temperature $T_{C,0}$ of the A-series samples; (c) enhancement of zero-resistance transition temperature $T_{C,0}$ of A-series samples, $\Delta T_{C,0}$; (d) normalized R–T curve of B-series samples; (e) zero-resistance transition temperature $T_{C,0}$ of the B-series samples; (f) enhancement of zero-resistance transition temperature $T_{C,0}$ of B-series samples, $\Delta T_{C,0}$.

Table 4 and Figure 5d show the critical transition temperature (T_C) and normalized R–T curves of the B-series samples prepared from raw material S2 with a particle size of 5 μm , as measured by the four-probe method. The gray curve in the figure represents the pure sample B1 of B(P)SCCO, with a transition temperature of 102–109 K. The remaining four curves represent the inhomogeneous phase-doped samples B2, B3, B4, and B5 with x wt.% ($x = 0.1, 0.15, 0.2$) content, with transition temperatures of 102.5–112, 103–112, 104–112 K, and 103.5–112 K, respectively. Figure 5e shows the zero-resistance transition temperature $T_{C,0}$ of the B-series samples. Figure 5f shows the enhancement of the zero-resistance temperature ($T_{C,0}$) in the B-series samples, denoted as $\Delta T_{C,0}$. It can be observed from the figure that the inhomogeneous phase doping effectively enhances the critical temperature T_C of the B(P)SCCO superconductor, with an increase of 3 K in the onset transition temperature $T_{C,on}$ and an enhancement of $\Delta T_{C,0}$ in the zero-resistance transition temperature $T_{C,0}$. The $\Delta T_{C,0}$ enhancement also shows a normal distribution relationship with the content of inhomogeneous phase doping. The optimal doping content is 0.2 wt.% and the zero-resistance transition temperature $T_{C,0}$ is increased by 2 K.

Table 4. Critical temperature (T_C) of B-series samples.

Samples	Concentration (wt.%)	$T_{C,0}/K$	$T_{C,on}/K$	$\Delta T_{C,0}/K$	$\Delta T_{C,on}/K$	Transition Width/K
B1	0	102 ± 0.17	109 ± 0.13	0	0	7
B2	0.1	102.5 ± 0.17	112 ± 0.14	0.5	3	9.5
B3	0.15	103 ± 0.15	112 ± 0.18	1	3	9
B4	0.2	104 ± 0.19	112 ± 0.17	2	3	8
B5	0.25	103.5 ± 0.13	112 ± 0.15	1.5	3	8.5

From Tables 3 and 4, and Figure 5, it can be seen that the critical temperature (T_C) of the A-series samples is higher than the T_C of the B-series samples. This is because the grain size of the B(P)SCCO samples prepared from raw materials with different particle sizes is different. The grain size of the B-series samples is smaller than that of the A-series samples, leading to an increase in grain boundaries and porosity within the B-series samples. This results in a decrease in connectivity between the grains and a decrease in the current-carrying capability between superconducting grains. As a result, the critical temperature T_C of the samples decreases [66,67]. However, the reduction in grain size and the increase in grain boundaries allow the B-series samples to accommodate more inhomogeneous phases. Therefore, we can see from the figure that the optimal doping concentration for the A-series samples is 0.15 wt.%, while the optimal doping concentration for the B-series samples is 0.2 wt.%, and the enhancement of the critical temperature T_C in the B-series samples is better than that in the A-series samples.

4.3. Critical Current Density J_C

Figure 6a,b show the relationship between the critical current density (J_C) and temperature (T) for the pure B(P)SCCO sample A1 and the inhomogeneous phase-doped B(P)SCCO samples A2, A3, and A4 with x wt.% ($x = 0.1, 0.15, 0.2$) content, prepared from raw material S1 with a particle size of 30 μm . Figure 6c,d show the relationship between J_C and T for the pure B(P)SCCO sample B1 and the inhomogeneous phase-doped samples B2, B3, and B4 with x wt.% ($x = 0.1, 0.15, 0.2$) content, prepared from raw material S2 with a particle size of 5 μm . These curves were obtained from I–V measurements. The critical current densities J_C of the pure B(P)SCCO samples at a temperature of 90 K were 105 A/cm² and 56 A/cm², respectively, which were consistent with the literature. From the graphs, it can be seen that J_C decreases with the increasing temperature, with a faster decrease in the low-temperature range and a slower decrease at higher temperatures. The J_C decreased to a minimum at the onset transition temperature $T_{C,on}$, consistent with the relationship between the critical current J_C and temperature T reported in the literature [68,69]. The increase in grain boundaries in the B-series samples prepared from smaller raw material sizes compared to the A-series samples led to poorer connectivity, resulting in a lower critical current density J_C for the B-series samples at the same temperature as the A-series samples [66,67]. In addition, from the graphs, it can be seen that, at the same temperature, the critical current density J_C of the inhomogeneous phase-doped samples is higher than that of the pure B(P)SCCO samples. The optimal doping content for the inhomogeneous phase in the A-series samples is 0.15 wt.%, and at a temperature of 90 K, the critical current density is increased by 25% compared to the pure B(P)SCCO sample. The optimal doping content for the inhomogeneous phase in the B-series samples is 0.2 wt.%, and at a temperature of 90 K, the critical current density J_C is increased by 35% compared to the pure B(P)SCCO sample. This indicates that inhomogeneous phase doping can effectively enhance the critical current density J_C of B(P)SCCO superconductors, and the smaller the grain size, the higher the content of inhomogeneous phase that can be accommodated, resulting in a better enhancement.

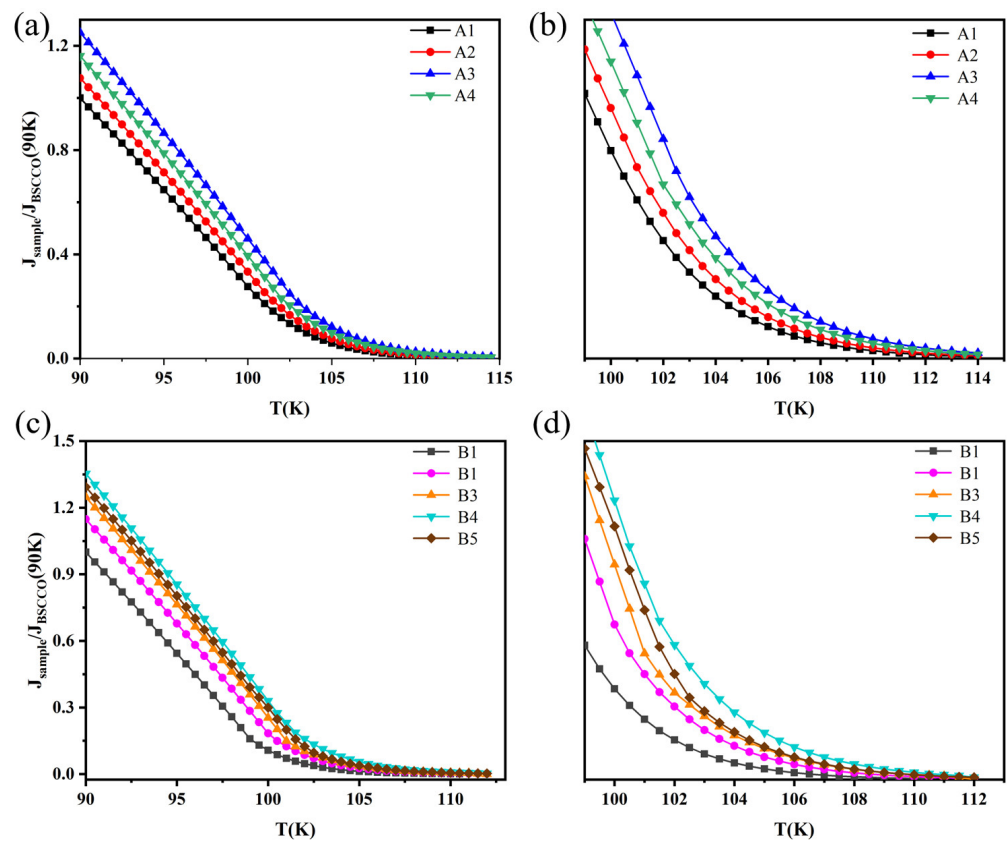


Figure 6. The relationship between critical current density (J_c) and temperature for A-series samples (a,b) and B-series samples (c,d); (b,d) are enlarged views of the local region.

4.4. Complete Diamagnetism (Meissner Effect)

Figure 7 shows the DC magnetization data for the A- and B-series samples. The horizontal axis represents the temperature and the vertical axis represents the percentage change in the material's complete diamagnetic response, expressed as the Meissner effect. From the DC magnetization data, it can be observed that all samples exhibit complete diamagnetism (Meissner effect). As the temperature increases, the complete diamagnetic response (Meissner effect) weakens and eventually disappears, consistent with the literature [70,71]. From Figure 7a, it can be seen that the complete diamagnetic response (Meissner effect) of the pure B(P)SCCO sample A1 completely disappears at 100.5 K, while for the inhomogeneous doped samples A2, A3, and A4 with doping contents of 0.1 wt.%, 0.15 wt.%, and 0.2 wt.%, the complete diamagnetic response (Meissner effect) disappears at temperatures of 101, 103, and 102.5 K, respectively. Figure 7b shows that at a temperature of 97 K, the complete diamagnetic response (Meissner effect) of the pure B(P)SCCO sample B1 completely disappears, while for the inhomogeneous phase-doped samples B2, B3, B4, and B5 with doping contents of 0.1 wt.%, 0.15 wt.%, 0.2 wt.%, and 0.25 wt.%, the complete diamagnetic response (Meissner effect) disappears at temperatures of 98, 99, 100, and 99 K, respectively. In both the A- and B-series samples, the inhomogeneous phase-doped samples exhibit an increased complete diamagnetic response (Meissner effect) compared to the pure B(P)SCCO samples, indicating that inhomogeneous phase doping effectively enhances the complete diamagnetic response (Meissner effect) of the B(P)SCCO samples.

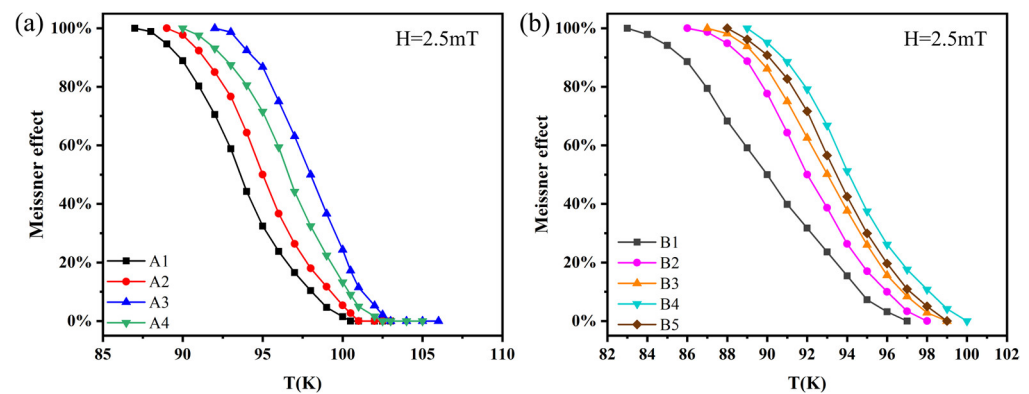


Figure 7. (a) DC magnetization data of A-series samples; (b) DC magnetization data of B-series samples.

5. Discussion

We introduced green-light-emitting GaN p-n junction particles as inhomogeneous phase inclusions into B(P)SCCO superconductors, forming smart meta-superconductors (SMSCs). We investigated the effect of the doping content of p-n junction luminescent particles on the superconducting properties of B(P)SCCO superconductors with different matrix sizes. The following points need further elaboration:

5.1. The Enhancement Effect of Green-Light p-n Junction Luminescent Particle Doping

Compared to pure B(P)SCCO samples, the doping of GaN p-n junction particles can indeed enhance the critical transition temperature (T_C), critical current (J_C), and perfect diamagnetism (Meissner effect) of B(P)SCCO superconductors, and the enhancement effect varies with the content of non-uniform phase doping in a dome-shaped manner. In the A-series samples, the doping of the inhomogeneous phase increased the zero-resistance transition temperature $T_{C,0}$ of the samples by 2 K and increased the critical current J_C by 25%; in the B-series samples, the doping of the inhomogeneous phase increased the zero-resistance transition temperature $T_{C,0n}$ by 3 K, increased the starting transition temperature $T_{C,0}$ by 2 K, and increased the critical current J_C by 35%.

5.2. Adjusting the Matrix Size of B(P)SCCO Superconductors Can Regulate the Enhancement Effect of Superconducting Properties

Comparing the A- and B-series samples, the particle size of the raw material decreased, resulting in smaller B(P)SCCO polycrystalline particle sizes. This led to an increase in the grain boundaries and porosity in the B-series samples, resulting in a lower critical temperature (T_C) and critical current (J_C) compared to the A-series samples [66,67]. In addition, for the A-series samples prepared from raw materials with a particle size of 30 μm , the optimal content of inhomogeneous phase doping was 0.15 wt.%, while for the B-series samples prepared from raw materials with a particle size of 5 μm , the optimal content was 0.2 wt.%, further enhancing the superconducting properties of B(P)SCCO superconductors. This indicates that, in our designed smart B(P)SCCO meta-superconductor structure, the smaller the particle size of the B(P)SCCO matrix, the more inhomogeneous phase content it can accommodate, resulting in a better performance enhancement.

5.3. Comparison of Chemical Doping and Luminescent Inhomogeneous Phase Doping

Chemical doping is a commonly used method to enhance superconducting properties. In previous studies, some researchers attempted to enhance the superconducting properties of BSCCO superconductors through element substitution. The most successful method to date is the substitution of Pb^{2+} for Bi^{3+} to enhance the stability of the Bi-2223 high-temperature phase and increase its content, but it cannot increase the critical temperature (T_C). Other elements, such as Al, Cs, and Ce, can only effectively increase the critical current density (J_C). Another group of researchers used compound doping, such as Al_2O_3 , SnO_2 ,

ZrO₂, and MgO. Studies have shown that compound doping can also only increase the critical current density (J_C). In this study, we introduced GaN p-n junction luminescent particles as inhomogeneous phase inclusions into B(P)SCCO superconductors. Through our experiments, we found that inhomogeneous phase doping simultaneously enhanced the critical temperature (T_C), critical current density (J_C), and complete diamagnetism of B(P)SCCO superconductors. Compared to chemical doping, which only increases the critical current density (J_C), this method has significant advantages. This method of enhancing superconductivity through the electroluminescence effect of luminescent particles provides a new approach to explore superconductor modification.

5.4. Universality of Enhancing Superconducting Performance through Luminescent Inhomogeneous Phase Doping

In previous experiments, our team introduced Y₂O₃:Eu³⁺ + Ag electroluminescent particles as inhomogeneous phase dopants into B(P)SCCO high-temperature superconductors to enhance their superconducting properties. The optimal doping content of Y₂O₃:Eu³⁺ + Ag electroluminescent particles was found to be 0.2 wt.%, which increased the zero-resistance transition temperature ($T_{C,0}$) by 1 K and the onset transition temperature ($T_{C,on}$) by 1.1 K compared to the same batch of pure B(P)SCCO superconductors [61,62]. At present, with green GaN p-n junction luminescent particles, the enhancement effect on the onset transition temperature ($\Delta T_{C,on}$) of the same batch of samples reached 2 K. It can be observed that the effect of these electroluminescent inhomogeneous phases is not significantly influenced by the material composition, but depends on their luminescent performance under an electric field. The use of electroluminescent inhomogeneous phase doping to improve superconducting performance is a universally existing phenomenon.

5.5. Enhancement Effect of p-n Junction Luminescent Particle Doping on Different Superconductors

We also introduced red AlGaInP p-n junction particles as inhomogeneous phase dopants into MgB₂ conventional superconductors, increasing the critical temperature to 39 K and $\Delta T_{C,on}$ to 0.8 K [64]. At present, with green GaN p-n junction luminescent particle doping in B(P)SCCO high-temperature superconductors, the critical transition temperature is also increased, and $\Delta T_{C,on}$ reaches 2 K. Whether for conventional or high-temperature superconductors, the use of p-n junction electroluminescent particle doping to enhance superconductivity is feasible and universal.

5.6. The Physical Origin of the Increase in the Critical Transition Temperature

Through the experiments, we observed that both Y₂O₃:Eu³⁺ + Ag rare-earth oxide luminescent particles and p-n junction luminescent particles, as inhomogeneous phase dopants in superconductors, could enhance the superconductivity to varying degrees [62,63]. However, there is currently no theoretical model that can explain this phenomenon well in accordance with experimental results. Therefore, based on years of experimental research, we proposed the idea that the coupling between the evanescent waves generated by electroluminescence and the superconducting electrons enhanced the critical transition temperature (T_C) of the superconductor [64]. By introducing p-n junction luminescent inhomogeneous phases, the photons generated by electroluminescent particles interacted with some superconducting electrons, resulting in the formation of surface plasmas. These evanescent waves promoted the smooth transmission of superconducting electrons with the same energy, thereby facilitating electron interactions in the surface plasma system. The injection of energy improved the formation of electron pairs, enhanced the superconducting behavior of the material, increased the critical transition temperature, and led to the formation of the superconductivity enhancement effect. At the same time, the incorporation of inhomogeneous phases can cause impurity effects, which, to some extent, disrupt the macroscopic superconductivity of the superconductor. There was obvious competition between the impurity effects caused by inhomogeneity and the excitation effects of electroluminescence. When the excitation effects of electroluminescence dominated,

the critical transition temperature increased ($\Delta T_C > 0$). Conversely, the introduction of inhomogeneity reduced the critical transition temperature ($\Delta T_C < 0$). Therefore, with the increase in the inhomogeneous phase content, the impurity effects were enhanced, and the enhancement of superconductivity exhibited a peak-shaped variation.

6. Conclusions

In this paper, we constructed B(P)SCCO smart meta-superconductors (SMSCs) by introducing green-light GaN p-n junction particles as inhomogeneous phases into B(P)SCCO superconducting particles. Two different series of samples were prepared using a solid-state sintering method with two different particle size raw materials. The critical temperature (T_C), critical current (J_C), and complete diamagnetism (Meissner effect) of the samples were measured using the four-probe method, I–V curve measurement, and DC magnetization measurement. The influence of introducing green-light GaN p-n junction inhomogeneous phases on the superconducting properties of B(P)SCCO samples was investigated. The experimental results show that by optimizing the doping of luminescent inhomogeneous phases, the critical transition temperature (T_C) can be increased by 3 K, the critical current density (J_C) can be increased by 35%, and the complete diamagnetism (Meissner effect) can be significantly enhanced. Through systematic studies, we found that the combination of electroluminescence and impurity effects caused by the traditional inhomogeneous doping phase could change the superconducting properties of superconductors. The stronger the electroluminescence effect of the luminescent inhomogeneous phases, the better the enhancement of the superconducting properties. This study provides valuable insights into and guidance for the optimization design and application of superconducting materials. Future research can further explore suitable doping materials with excellent performances and investigate the physical mechanisms of enhancing superconducting properties, thus further promoting the exploration and application of superconducting materials.

Author Contributions: Conceptualization and methodology, X.Z.; software, Q.H., H.C. and D.C.; validation, Q.H., H.C. and C.S.; formal analysis, Q.H., H.C., C.S., D.C., Y.Q. and M.S.; investigation, Q.H., H.C., C.S., D.C., Y.Q. and M.S.; resources, X.Z.; data curation, Q.H., H.C. and C.S.; writing—original draft preparation, Q.H.; writing—review and editing, Q.H. and X.Z.; visualization, Q.H., Y.Q. and M.S.; supervision, X.Z.; project administration, X.Z.; funding acquisition, X.Z. All authors have read and agreed to the published version of the manuscript.

Funding: This research was supported by the National Natural Science Foundation of China for Distinguished Young Scholars under Grant No. 50025207.

Data Availability Statement: The data presented in this study are available on reasonable request from the corresponding author.

Conflicts of Interest: The authors declare no conflict of interest.

References

1. Bardeen, J.; Cooper, L.N.; Schrieffer, J.R. Theory of Superconductivity. *Phys. Rev.* **1957**, *108*, 1175–1204. [[CrossRef](#)]
2. Bardeen, J. Theory of the Meissner Effect in Superconductors. *Phys. Rev.* **1955**, *97*, 1724–1725. [[CrossRef](#)]
3. Bednorz, J.G.; Müller, K.A. Possible high T_C superconductivity in the Ba-La-Cu-O system. *Z. Phys. B Condens. Matter* **1986**, *64*, 189–193. [[CrossRef](#)]
4. Agterberg, D.F.; Davis, J.S.; Edkins, S.D.; Fradkin, E.; Van Harlingen, D.J.; Kivelson, S.A.; Lee, P.A.; Radzihovsky, L.; Tranquada, J.M.; Wang, Y. The Physics of Pair-Density Waves: Cuprate Superconductors and Beyond. *Annu. Rev. Condens. Matter Phys.* **2020**, *11*, 231–270. [[CrossRef](#)]
5. Kamihara, Y.; Watanabe, T.; Hirano, M.; Hosono, H. Iron-Based Layered Superconductor $\text{La}[\text{O}_{1-x}\text{F}_x]\text{FeAs}$ ($x = 0.05\text{--}0.12$) with $T_C = 26$ K. *J. Am. Chem. Soc.* **2008**, *130*, 3296–3297. [[CrossRef](#)]
6. Chen, X.H.; Dai, P.C.; Feng, D.L.; Xiang, T.; Zhang, F.C. Iron-based high transition temperature superconductors. *Natl. Sci. Rev.* **2014**, *1*, 371–395. [[CrossRef](#)]
7. Zhang, P.; Yaji, K.; Hashimoto, T.; Ota, Y.; Kondo, T.; Okazaki, K.; Wang, Z.; Wen, J.; Gu, G.D.; Ding, H.; et al. Observation of topological superconductivity on the surface of an iron-based superconductor. *Science* **2018**, *360*, 182–186. [[CrossRef](#)]
8. Drozdov, A.P.; Erements, M.I.; Troyan, I.A.; Ksenofontov, V.; Shylin, S.I. Conventional superconductivity at 203 kelvin at high pressures in the sulfur hydride system. *Nature* **2015**, *525*, 73–76. [[CrossRef](#)]

9. Drozdov, A.P.; Kong, P.P.; Minkov, V.S.; Besedin, S.P.; Kuzovnikov, M.A.; Mozaffari, S.; Balicas, L.; Balakirev, F.F.; Graf, D.E.; Prakapenka, V.B.; et al. Superconductivity at 250 K in lanthanum hydride under high pressures. *Nature* **2019**, *569*, 528–531. [[CrossRef](#)]
10. Sun, W.G.; Kuang, X.Y.; Keen, H.D.J.; Lu, C.; Hermann, A. Second group of high-pressure high-temperature lanthanide polyhydride superconductors. *Phys. Rev. B* **2020**, *102*, 144524. [[CrossRef](#)]
11. Dasenbrock-Gammon, N.; Snider, E.; McBride, R.; Pasan, H.; Durkee, D.; Khalvashi-Sutter, N.; Munasinghe, S.; Dissanayake, S.E.; Lawler, K.V.; Salamat, A.; et al. Evidence of near-ambient superconductivity in a N-doped lutetium hydride. *Nature* **2023**, *615*, 244–250. [[CrossRef](#)] [[PubMed](#)]
12. Kaiser, S.; Hunt, C.R.; Nicoletti, D.; Hu, W.; Gierz, I.; Liu, H.Y.; Le Tacon, M.; Loew, T.; Haug, D.; Keimer, B.; et al. Optically induced coherent transport far above T_C in underdoped $\text{YBa}_2\text{Cu}_3\text{O}_{6+\delta}$. *Phys. Rev. B* **2014**, *89*, 184516. [[CrossRef](#)]
13. Mitrano, M.; Cantaluppi, A.; Nicoletti, D.; Kaiser, S.; Perucchi, A.; Lupi, S.; Di Pietro, P.; Pontiroli, D.; Riccò, M.; Clark, S.R.; et al. Possible light-induced superconductivity in K_3C_{60} at high temperature. *Nature* **2016**, *530*, 461–464. [[CrossRef](#)] [[PubMed](#)]
14. Cantaluppi, A.; Buzzi, M.; Jotzu, G.; Nicoletti, D.; Mitrano, M.; Pontiroli, D.; Riccò, M.; Perucchi, A.; Di Pietro, P.; Cavalleri, A. Pressure tuning of light-induced superconductivity in K_3C_{60} . *Nat. Phys.* **2018**, *14*, 837–841. [[CrossRef](#)] [[PubMed](#)]
15. Saito, Y.; Kasahara, Y.; Ye, J.T.; Iwasa, Y.; Nojima, T. Metallic ground state in an ion-gated two-dimensional superconductor. *Science* **2015**, *350*, 409–413. [[CrossRef](#)]
16. Saito, Y.; Nojima, T.; Iwasa, Y. Highly crystalline 2D superconductors. *Nat. Rev. Mater.* **2017**, *2*, 16094. [[CrossRef](#)]
17. Zhou, H.X.; Xie, T.; Taniguchi, T.; Watanabe, K.; Young, A.F. Superconductivity in rhombohedral trilayer graphene. *Nature* **2021**, *598*, 434–438. [[CrossRef](#)]
18. Richter, C.; Boschker, H.; Dietsche, W.; Fillis-Tsirakis, E.; Jany, R.; Loder, F.; Kourkoutis, L.F.; Muller, D.A.; Kirtley, J.R.; Schneider, C.W.; et al. Interface superconductor with gap behaviour like a high-temperature superconductor. *Nature* **2013**, *502*, 528–531. [[CrossRef](#)]
19. Tan, S.; Zhang, Y.; Xia, M.; Ye, Z.; Chen, F.; Xie, X.; Peng, R.; Xu, D.; Fan, Q.; Xu, H.; et al. Interface-induced superconductivity and strain-dependent spin density waves in $\text{FeSe}/\text{SrTiO}_3$ thin films. *Nat. Mater.* **2013**, *12*, 634–640. [[CrossRef](#)]
20. Chen, Z.; Liu, Y.; Zhang, H.; Liu, Z.; Tian, H.; Sun, Y.; Zhang, M.; Zhou, Y.; Sun, J.; Xie, Y. Electric field control of superconductivity at the $\text{LaAlO}_3/\text{KTaO}_3(111)$ interface. *Science* **2021**, *372*, 721–724. [[CrossRef](#)]
21. Li, D.; Lee, K.; Wang, B.Y.; Osada, M.; Crossley, S.; Lee, H.R.; Cui, Y.; Hikita, Y.; Hwang, H.Y. Superconductivity in an infinite-layer nickelate. *Nature* **2019**, *572*, 624–627. [[CrossRef](#)] [[PubMed](#)]
22. Ding, X.; Tam, C.C.; Sui, X.; Zhao, Y.; Xu, M.; Choi, J.; Leng, H.; Zhang, J.; Wu, M.; Xiao, H.; et al. Critical role of hydrogen for superconductivity in nickelates. *Nature* **2023**, *615*, 50–55. [[CrossRef](#)] [[PubMed](#)]
23. Sun, H.; Huo, M.; Hu, X.; Li, J.; Liu, Z.; Han, Y.; Tang, L.; Mao, Z.; Yang, P.; Wang, B.; et al. Signatures of superconductivity near 80 K in a nickelate under high pressure. *Nature* **2023**, *621*, 493–498. [[CrossRef](#)] [[PubMed](#)]
24. Malozemoff, A.P. Second-Generation High-Temperature Superconductor Wires for the Electric Power Grid. *Annu. Rev. Mater. Res.* **2012**, *42*, 373–397. [[CrossRef](#)]
25. Mukherjee, P.; Rao, V.V. Superconducting magnetic energy storage for stabilizing grid integrated with wind power generation systems. *J. Mod. Power Syst. Clean Energy* **2019**, *7*, 400–411. [[CrossRef](#)]
26. Yao, C.; Ma, Y.W. Superconducting materials: Challenges and opportunities for large-scale applications. *Iscience* **2021**, *24*, 102541. [[CrossRef](#)] [[PubMed](#)]
27. Sorbom, B.; Ball, J.; Palmer, T.; Mangiarotti, F.; Sierchio, J.; Bonoli, P.; Kasten, C.; Sutherland, D.; Barnard, H.; Haakonsen, C.; et al. ARC: A compact, high-field, fusion nuclear science facility and demonstration power plant with demountable magnets. *Fusion Eng. Des.* **2015**, *100*, 378–405. [[CrossRef](#)]
28. Nayak, C.; Simon, S.H.; Stern, A.; Freedman, M.; Das Sarma, S. Non-Abelian anyons and topological quantum computation. *Rev. Mod. Phys.* **2008**, *80*, 1083–1159. [[CrossRef](#)]
29. Qi, X.L.; Hughes, T.L.; Zhang, S.C. Chiral topological superconductor from the quantum Hall state. *Phys. Rev. B* **2010**, *82*, 184516. [[CrossRef](#)]
30. Fornieri, A.; Whitticar, A.M.; Setiawan, F.; Portolés, E.; Drachmann, A.C.C.; Keselman, A.; Gronin, S.; Thomas, C.; Wang, T.; Kallagher, R.; et al. Evidence of topological superconductivity in planar Josephson junctions. *Nature* **2019**, *569*, 89–92. [[CrossRef](#)]
31. Grilli, F.; Pardo, E.; Stenvall, A.; Nguyen, D.N.; Yuan, W.; Gomory, F. Computation of Losses in HTS under the Action of Varying Magnetic Fields and Currents. *IEEE Trans. Appl. Supercond.* **2014**, *24*, 78–110. [[CrossRef](#)]
32. Shen, B.Y.; Grilli, F.; Coombs, T. Review of the AC loss computation for HTS using H formulation. *Supercond. Sci. Technol.* **2020**, *33*, 033002. [[CrossRef](#)]
33. Pan, X.Y.; Wu, W.; Yu, X.; Lu, L.; Guo, C.J.; Zhao, Y. Typical electrical, mechanical, electromechanical characteristics of copper-encapsulated REBCO tapes after processing in temperature under 250 °C. *Supercond. Sci. Technol.* **2023**, *36*, 034004. [[CrossRef](#)]
34. Weber, H.W. Radiation Effects on Superconducting Fusion Magnet Components. *Int. J. Mod. Phys. E* **2011**, *20*, 1325–1378. [[CrossRef](#)]
35. Haran, K.S.; Kalsi, S.; Arndt, T.; Karmaker, H.; Badcock, R.; Buckley, B.; Haugan, T.; Izumi, M.; Loder, D.; Bray, J.W.; et al. High power density superconducting rotating machines-development status and technology roadmap. *Supercond. Sci. Technol.* **2017**, *30*, 123002. [[CrossRef](#)]

36. Hosono, H.; Yamamoto, A.; Hiramatsu, H.; Ma, Y.W. Recent advances in iron-based superconductors toward applications. *Mater. Today* **2018**, *21*, 278–302. [[CrossRef](#)]
37. Dai, P.C. Antiferromagnetic order and spin dynamics in iron-based superconductors. *Rev. Mod. Phys.* **2015**, *87*, 855–896. [[CrossRef](#)]
38. Tallon, L.J.; Buckley, G.R.; Gilbert, W.P.; Presland, R.M.; Brown, M.W.I.; Bowder, E.M.; Christian, A.L.; Gafull, R. High-TC superconducting phases in the series $\text{Bi}_{2.1}(\text{Ca}, \text{Sr})_{n+1}\text{Cu}_n\text{O}_{2n+4+\delta}$. *Nature* **1988**, *333*, 153–156. [[CrossRef](#)]
39. Majewsky, P.; Hettich, B.; Schulze, K.; Petzow, G. Preparation of unleaded $\text{Bi}_2\text{Sr}_2\text{Ca}_2\text{Cu}_3\text{O}_{10}$. *Adv. Mater.* **1991**, *3*, 488–491. [[CrossRef](#)]
40. Ikeda, Y.; Takano, M.; Hiroi, Z.; Oda, K.; Kitaguchi, H.; Takada, J.; Miura, Y.; Takeda, Y.; Yamamoto, O.; Mazaki, H. The High-TC Phase with a New Modulation Mode in the Bi, Pb-Sr-Ca-Cu-O System. *Jpn. J. Appl. Phys.* **1988**, *27*, L2067–L2070. [[CrossRef](#)]
41. Asghari, R.; Naghshara, H.; Arsalan, L.C.; Sedghi, H. Comparing the Effects of Nb, Pb, Y, and La Replacement on the Structural, Electrical, and Magnetic Characteristics of Bi-Based Superconductors. *J. Supercond. Nov. Magn.* **2018**, *31*, 3889–3898. [[CrossRef](#)]
42. Honma, T.; Hor, P.H. Universal optimal hole-doping concentration in single-layer high-temperature cuprate superconductors. *Supercond. Sci. Technol.* **2006**, *19*, 907–911. [[CrossRef](#)]
43. Tsui, O.K.C.; Ong, N.P.; Peterson, J.B. Excitation of the Josephson plasma mode in $\text{Bi}_2\text{Sr}_2\text{CaCu}_2\text{O}_{8+\delta}$ in an oblique field. *Phys. Rev. Lett.* **1996**, *76*, 819–822. [[CrossRef](#)] [[PubMed](#)]
44. Murakami, H.; Kiwa, T.; Misra, M.; Tonouchi, M.; Uchiyama, T.; Iguchi, I.; Wang, Z. Terahertz pulse radiation properties of a $\text{Bi}_2\text{Sr}_2\text{CaCu}_2\text{O}_{8+\delta}$ bowtie antenna by optical pulse illumination. *Jpn. J. Appl. Phys. Part 1-Regul. Pap. Brief Commun. Rev. Pap.* **2002**, *41*, 1992–1997. [[CrossRef](#)]
45. Kawayama, I.; Zhang, C.H.; Wang, H.B.; Tonouchi, M. Study on terahertz emission and optical/terahertz pulse responses with superconductors. *Supercond. Sci. Technol.* **2013**, *26*, 093002. [[CrossRef](#)]
46. Hudakova, N.; Plechacek, V.; Dordor, P.; Flachbart, K.; Knizek, K.; Kovac, J.; Reiffers, M. Influence of Pb concentration on microstructural and superconducting properties of BSCCO superconductors. *Supercond. Sci. Technol.* **1995**, *8*, 324–328. [[CrossRef](#)]
47. Chu, C.W.; Bechtold, J.; Gao, L.; Hor, P.H.; Huang, Z.J.; Meng, R.L.; Sun, Y.Y.; Wang, Y.Q.; Xue, Y.Y. Superconductivity up to 114 K in the Bi-Al-Ca-Sr-Cu-O compound system without rare-earth elements. *Phys. Rev. Lett.* **1988**, *60*, 941–943. [[CrossRef](#)] [[PubMed](#)]
48. Zhigadlo, N.D.; Petrashko, V.V.; Semenenko, Y.A.; Panagopoulos, C.; Cooper, J.R.; Salje, E.K.H. The effects of Cs doping, heat treatments on the phase formation and superconducting properties of (Bi, Pb)-Sr-Ca-Cu-O ceramics. *Phys. C Supercond.* **1998**, *299*, 327–337. [[CrossRef](#)]
49. Jordan, F.; Pena, O. Texturation and critical currents in cerium-substituted cuprates $\text{Bi}_2\text{Sr}_2\text{Ca}_{1-x}\text{Ce}_x\text{Cu}_2\text{O}_{8+\delta}$. *J. Magn. Magn. Mater.* **1995**, *140*, 1315–1316. [[CrossRef](#)]
50. Annabi, M.; M'Chirgui, A.; Ben Azzouz, F.; Zouaoui, M.; Ben Salem, M. Addition of nanometer Al_2O_3 during the final processing of (Bi,Pb)-2223 superconductors. *Phys. C-Supercond. Its Appl.* **2004**, *405*, 25–33. [[CrossRef](#)]
51. Yavuz, Ş.; Bilgili, Ö.; Kocabaş, K. Effects of superconducting parameters of SnO_2 nanoparticles addition on (Bi, Pb)-2223 phase. *J. Mater. Sci. Mater. Electron.* **2016**, *27*, 4526–4533. [[CrossRef](#)]
52. Jia, Z.Y.; Tang, H.; Yang, Z.Q.; Xing, Y.T.; Wang, Y.Z.; Qiao, G.W. Effects of nano- ZrO_2 particles on the superconductivity of Pb-doped BSCCO. *Phys. C* **2000**, *337*, 130–132. [[CrossRef](#)]
53. Guilmeau, E.; Andrzejewski, B.; Noudem, J.G. The effect of MgO addition on the formation and the superconducting properties of the Bi2223 phase. *Phys. C-Supercond. Its Appl.* **2003**, *387*, 382–390. [[CrossRef](#)]
54. Zhao, Q.; Zhao, X.P.; Kang, L.; Zhang, F.L.; Liu, Y.H.; Luo, C.R. The defect effect in the one-dimensional negative permeability material. *Acta Phys. Sin.* **2004**, *53*, 2206–2211. [[CrossRef](#)]
55. Zhao, X. Bottom-up fabrication methods of optical metamaterials. *J. Mater. Chem.* **2012**, *22*, 9439–9449. [[CrossRef](#)]
56. Smolyaninova, V.N.; Yost, B.; Zander, K.; Osofsky, M.S.; Kim, H.; Saha, S.; Greene, R.L.; Smolyaninov, I.I. Experimental demonstration of superconducting critical temperature increase in electromagnetic metamaterials. *Sci. Rep.* **2014**, *4*, 7321. [[CrossRef](#)] [[PubMed](#)]
57. Zhang, Z.W.; Tao, S.; Chen, G.W.; Zhao, X.P. Improving the Critical Temperature of MgB_2 Superconducting Metamaterials Induced by Electroluminescence. *J. Supercond. Nov. Magn.* **2016**, *29*, 1159–1162. [[CrossRef](#)]
58. Tao, S.; Li, Y.B.; Chen, G.W.; Zhao, X.P. Critical Temperature of Smart Meta-superconducting MgB_2 . *J. Supercond. Nov. Magn.* **2017**, *30*, 1405–1411. [[CrossRef](#)]
59. Li, Y.B.; Chen, H.G.; Wang, M.Z.; Xu, L.X.; Zhao, X.P. Smart meta-superconductor MgB_2 constructed by the dopant phase of luminescent nanocomposite. *Sci. Rep.* **2019**, *9*, 14194. [[CrossRef](#)]
60. Li, Y.B.; Han, G.Y.; Zou, H.Y.; Tang, L.; Chen, H.G.; Zhao, X.P. Reinforcing Increase of ΔT_C in MgB_2 Smart Meta-Superconductors by Adjusting the Concentration of Inhomogeneous Phases. *Materials* **2021**, *14*, 3066. [[CrossRef](#)]
61. Chen, H.G.; Li, Y.B.; Wang, M.Z.; Han, G.Y.; Shi, M.; Zhao, X.P. Smart meta-structure method for increasing T_C of Bi(Pb)SrCaCuO high-temperature superconductors. *J. Supercond. Nov. Magn.* **2020**, *33*, 3015–3025. [[CrossRef](#)]
62. Chen, H.G.; Wang, M.Z.; Qi, Y.; Li, Y.B.; Zhao, X.P. Relationship between the T_C of Smart Meta-Superconductor Bi(Pb)SrCaCuO and Inhomogeneous Phase Content. *Nanomaterials* **2021**, *11*, 1061. [[CrossRef](#)] [[PubMed](#)]
63. Chen, H.G.; Li, Y.B.; Qi, Y.; Wang, M.Z.; Zou, H.Y.; Zhao, X.P. Critical Current Density and Meissner Effect of Smart Meta-Superconductor MgB_2 and Bi(Pb)SrCaCuO. *Materials* **2022**, *15*, 972. [[CrossRef](#)] [[PubMed](#)]
64. Zhao, X.; Hai, Q.; Shi, M.; Chen, H.; Li, Y.; Qi, Y. An Improved Smart Meta-Superconductor MgB_2 . *Nanomaterials* **2022**, *12*, 2590. [[CrossRef](#)] [[PubMed](#)]

65. Wang, M.Z.; Xu, L.X.; Chen, G.W.; Zhao, X.P. Topological Luminophor $\text{Y}_2\text{O}_3:\text{Eu}^{3+}+\text{Ag}$ with High Electroluminescence Performance. *ACS Appl. Mater. Interfaces* **2019**, *11*, 2328–2335. [[CrossRef](#)]
66. Malik, B.A.; Rather, G.H.; Asokan, K.; Malik, M.A. Study on excess conductivity in YBCO + xAg composites. *Appl. Phys. A-Mater. Sci. Process.* **2021**, *127*, 294. [[CrossRef](#)]
67. Kamar, A.; Srouf, A.; Roumié, M.; Malaeb, W.; Awad, R.; Khalaf, A. Comparative study of structural and superconducting properties of $(\text{Cu}_{0.5}\text{Tl}_{0.5})\text{Ba}_2\text{Ca}_2\text{Cu}_3\text{O}_{10-\delta}$ phase substituted by copper fluoride and thallium fluoride. *Appl. Phys. A-Mater. Sci. Process.* **2021**, *127*, 579. [[CrossRef](#)]
68. Karaca, I.; Celebi, S.; Varilci, A.; Malik, A.I. Effect of Ag_2O addition on the intergranular properties of the superconducting Bi-(Pb)-Sr-Ca-Cu-O system. *Supercond. Sci. Technol.* **2003**, *16*, 100–104. [[CrossRef](#)]
69. Shamsodini, M.; Salamati, H.; Shakeripour, H.; Sarsari, I.A.; Esferizi, M.F.; Nikmanesh, H. Effect of using two different starting materials (nitrates and carbonates) and a calcination processes on the grain boundary properties of a BSCCO superconductor. *Supercond. Sci. Technol.* **2019**, *32*, 075001. [[CrossRef](#)]
70. Posselt, H.; Muller, H.; Andres, K.; Saito, G. Reentrant Meissner effect in the organic conductor $\kappa\text{-(BEDT-TTF)}_2\text{Cu}[\text{N}(\text{CN})_2]\text{Cl}$ under pressure. *Phys. Rev. B* **1994**, *49*, 15849–15852. [[CrossRef](#)]
71. Horiuchi, T.; Kawai, T.; Kawai, S.; Ogura, K. The trial of making Bi-Sr-Ca-Cu-M-O superconductors (M = Li, Na, K, Rb, Cs). *Ferroelectrics* **1990**, *109*, 351–356. [[CrossRef](#)]

Disclaimer/Publisher’s Note: The statements, opinions and data contained in all publications are solely those of the individual author(s) and contributor(s) and not of MDPI and/or the editor(s). MDPI and/or the editor(s) disclaim responsibility for any injury to people or property resulting from any ideas, methods, instructions or products referred to in the content.